

Role of Extracellular Domain Dimerization in Agonist-Induced Activation of Natriuretic Peptide Receptor-A

Marie Parat, Normand McNicoll, Brian Wilkes, Alain Fournier, and André De Léan

Department of Pharmacology, Faculty of Medicine, Université de Montréal (M.P., N.M.N., A.D.L.); Clinical Research Institute of Montreal, Université de Montréal (B.W.); INRS-IAF, Institut National de la Recherche Scientifique, Université du Québec (A.F.).

Running title: Dimerization of NPRA Extracellular Domain

Corresponding author: André De Léan, Department of Pharmacology, Faculty of Medicine, Université de Montréal, 2900 boulevard Édouard-Montpetit, Pavillon Principal, V437-1, Montréal, Québec, Canada H3T 1J4. Tel.: 514-343-6931. Fax: 514-343-2291. Email: delean@pharmco.umontreal.ca.

Number of pages: 42

Number of tables: 3

Number of figures: 7

Number of references: 40

Number of words in Abstract: 248

Number of words in Introduction: 748

Number of words in Discussion: 886

Abbreviations: A-71915, (Arg⁶, β -cyclohexyl-Ala⁸, D-Tic¹⁶, Arg¹⁷, Cys¹⁸)-rANP-(6-18)-amide; ANP, atrial natriuretic peptide; Atriopeptin II, rANP-(5-27); BANP, (Arg¹⁰, Leu¹², Ser¹⁷, Leu¹⁸)-rANP-(1-28); C-ANF, (Des-Gln¹⁸,des-Ser¹⁹,des-Gly^{20,22},des-Leu²¹)-rANP-(4-23)-amide; CD, cytoplasmic domain; CNP, C-Type natriuretic peptide; ECD, extracellular domain; FRET, fluorescence resonance energy transfer; AF488, Alexa Fluor 488; GC, guanylyl cyclase domain; GH, growth hormone; GHR, growth hormone receptor; IFNAR, Type I interferon receptor; KHD, kinase homology domain; mini-ANP, (Met⁵,Cys^{6,17},His⁷,Ser¹⁶,Tyr¹⁸,Arg¹⁹)-rANP-(5-19)-amide; MOI, multiplicity of infection; NPRA, natriuretic peptide receptor A; NPRB, natriuretic peptide receptor B; NPRC, natriuretic peptide receptor C; NP, natriuretic peptide; pBNP32, porcine brain natriuretic peptide-32; QMA, quaternary methyl ammonium; rANP, rat atrial natriuretic peptide 1-28; TCEP, Tris(2-Carboxyethyl) phosphine ; TM, transmembrane domain.

Abstract

Natriuretic peptide receptor A (NPRA) is composed of an extracellular domain (ECD) with a ligand binding site, a single transmembrane region, a kinase homology domain and a guanylyl cyclase domain. The natural agonists atrial and brain natriuretic peptides (ANP, BNP) bind and activate NPRA, leading to cyclic GMP production, responsible for their role in cardiovascular homeostasis. Previous studies suggested that stabilization of a dimeric form of NPRA by agonist is essential for receptor activation. However, ligand specificity and sequential steps of this dimerization process have not been investigated. We used radioligand binding, FRET homoquenching and molecular modeling to characterize the interaction of human NPRA-ECD with ANP, BNP, the superagonist BANP, the minimized analog mini-ANP and the antagonist A71915. ANP binds to preformed ECD dimers and spontaneous dimerization is the rate limiting step of the ligand binding process. All the studied peptides, including A71915 antagonist, induce a dose-dependent fluorescence homoquenching, specific to dimerization, with potencies highly correlated with their binding affinities. A71915 induced more quenching than other peptides, suggesting stabilization by the antagonist of ECD dimer in a distinct inactive conformation. In summary, these results indicate that the ligand-induced dimerization process of NPRA is different from that for cytokine receptor model. Agonists or antagonists bind to preformed dimeric ECD, leading to dimer stabilization in an active or inactive conformation, respectively. Furthermore, the highly-sensitive fluorescence assay designed to assess dimerization could serve as a powerful tool for further detailing the kinetic steps involved in natriuretic peptide receptor binding and activation.

Introduction

Natriuretic peptides provide an essential counterbalance mechanism to the renin-angiotensin-aldosterone system (Gardner et al., 2007). Their cardioprotective role is exemplified in gene knockout studies which have shown that they act locally to prevent cardiac hypertrophy (Kuhn, 2004). Gene polymorphism of atrial natriuretic peptide (ANP) and of natriuretic peptide receptor type-A (NPRA) has been associated with increased left ventricular mass in essential hypertensive patients (Rubattu et al., 2006). Natriuretic peptides are currently used as therapeutic agents in the treatment of the acute phase of myocardial infarct (Strain, 2004; Lee and Burnett Jr, 2007).

ANP cellular action is mediated through NPRA. This receptor is typical of membrane guanylyl cyclases and is formed of five domains (Padayatti et al., 2004). An extracellular domain (ECD) specifically binds natriuretic peptides in a 2:1 stoichiometric ratio (Rondeau et al., 1995; He et al., 2001; Ogawa et al., 2004). A single transmembrane (TM) domain transfers the activation conformational change from the ECD to the cytoplasmic domain (CD). The CD includes a kinase homology domain (KHD), which allosterically regulates both peptide binding to the ECD and activation of the effector guanylyl cyclase (GC) (Larose et al., 1991; Duda et al., 2004). The KHD directly binds ATP following activation of the ECD by ANP (Joubert et al., 2005). It is also normally phosphorylated and its dephosphorylation coincides with desensitization of NPRA to ANP activation (Potter et al., 2006; Joubert et al., 2001). The KHD and the GC domains are connected by a coiled-coil which maintains the catalytic moieties in close contact. The GC domain presents two functional and allosterically regulated catalytic sites whose structure is jointly contributed by both subunits (Joubert et al., 2007).

The extracellular juxtamembrane region connecting the bilobed ECD to the TM appears to play a crucial role in the transmembrane signal transduction mechanism. Mutation C423S disrupts a short intrachain disulfide-bridged loop and leads to constitutive activation of NPRA (Labrecque et al., 1999). The unpaired Cys⁴³² of this mutant forms an interchain disulfide, showing that the juxtamembrane regions are juxtaposed. However, mutation D435C, three residues downstream of Cys⁴³², leads to an agonist-induced disulfide, indicating that a conformational change, either a translation or a rotation of the subunits, is occurring upon activation by ANP (Labrecque et al., 2001). Crystallographic study of the soluble ECD of NPRA has confirmed this hypothesis (Ogawa et al., 2004), although no structural documentation of the juxtamembrane region of the ECD was obtained.

The cytokine receptor family displays structural similarities with those of natriuretic peptide receptors. The prototypical growth hormone receptor (GHR) is a homodimeric receptor constituted of an ECD with limited dimerization interface, but specific binding surfaces for contacting GH, a single transmembrane domain, and a cytoplasmic domain involved in activation of downstream effectors signalling (de Vos et al., 1992). For this hormone and for all cytokines, a site I on the agonist interacts sequentially with one receptor subunit (Cunningham et al., 1991). This first contact is followed by the interaction of site II of the ligand with a second receptor subunit, resulting in a more stable complex and in transmembrane activation (Cunningham and Wells, 1993). GH analogs mutated on site II fail to bind to the second receptor subunit and act as antagonists (Fuh et al., 1992). In addition, native GH at high concentration binds in a 1:1 stoichiometric ratio, resulting in a bell-shaped dose-response curve for GH (Cunningham et al., 1991).

In contrast with cytokines, ANP is not well structured in solution (Carpenter et al., 1997). However in the receptor-bound state it displays a flat ring moiety tightly interfacing with both ECD subunits, resulting in high affinity binding (Ogawa et al., 2004). Whether NPRA ECD is spontaneously monomeric or dimeric in the inactive state is still debated. It has been reported that the soluble ECD of NPRA is monomeric even at micromolar concentration and that it dimerizes only in the presence of ANP (Misono et al., 1999). However the sequence of the binding steps of ANP was not defined. We have studied by radioligand binding, FRET homotransfer and molecular modeling the interaction of NPRA ECD with the agonists rANP and pBNP, the superagonist BANP (Mimeault et al., 1993; Bodart et al., 1996), the minimized analog mini-ANP (Li et al., 1995) and the antagonist A71915 (von Geldern et al., 1990). The results indicate that ANP binds to preformed ECD dimers and that spontaneous ECD dimerization is the rate limiting step. In addition, we document that both agonists and the antagonist stabilize the ECD dimeric state, but with different conformations.

Materials and Methods

Materials

Rat Atrial Natriuretic Peptide 1-28 (rANP 1-28) and C-Type Natriuretic peptide (CNP) were purchased from Sigma-Aldrich (Saint-Louis, MO). (Arg⁶, b-cyclohexyl-Ala⁸, D-Tic¹⁶, Arg¹⁷, Cys¹⁸)-rANP-(6-18)-amide (A-71915), (Met⁵,Cys^{6,17},His⁷,Ser¹⁶,Tyr¹⁸,Arg¹⁹)-rANP-(5-19) amide (Mini-ANP), porcine Brain Natriuretic Peptide-32 (pBNP32) and (Des-Gln¹⁸,des-Ser¹⁹,des-Gly^{20,22},des-Leu²¹)-rANP-(4-23)-amide (C-ANF) were obtained from Bachem (Torrance, CA). (Arg¹⁰, Leu¹², Ser¹⁷, Leu¹⁸)-rANP-(1-28) (BANP or pBNP1) was synthesized as described (Mimeault et al., 1993). Aprotinin, Leupeptin, Pefabloc and Pepstatin were purchased from Roche Diagnostics (Laval, Canada). Oligonucleotides were obtained from BioCorp (Montréal, Canada).

Construction of Soluble hNPRA-ECD WT and C423S Mutant

Human full length NPRA clone, formerly inserted into the expression vector pBK-CMV (Stratagene, LaJolla, CA) (Jossart et al., 2005), was used for the construction of deletion mutants containing only the soluble extracellular domain (hNPRA-ECD). A carboxy-terminal His-Tag epitope (RSHHHHHH) was inserted by PCR mutagenesis at the membrane-proximal end of the extracellular domain of hNPRA, beginning at and replacing residue Glu⁴⁴¹ (mature protein numbering), as described for the rat NPRA (Labrecque et al., 1999). The hNPRA-ECD^{WT} truncation mutant was subcloned into the SF9 cell expression vector pFastBac1 (Invitrogen, Burlington, Canada). In order to improve the expression level of the secreted ECD by Sf9 cells, the hNPRA peptide signal was substituted with the melittin peptide signal MKFLVNVALVFMVVYISYIYA, using a synthetic DNA linker replacing the signal peptide up

to the first mature residue Gly¹. The disulfide-bridged hNPRA-ECD^{C423S} mutant was obtained by site-directed mutagenesis, using the QuikChange methodology (Stratagene, LaJolla, CA), as described previously (Labrecque et al., 1999).

Transfection of Sf9 Insect Cells

Sf9 cells were grown in SF-900 II SFM medium (Invitrogen, Burlington, Canada) containing penicillin and streptomycin on a rotating shaker at 28°C. For each transfection, 9×10^5 cells were seeded in a 6-well plate and allowed to attach for at least 1 h. Recombinant Bacmid DNA was transfected into Sf9 insect cells using Cellfectin reagent (Invitrogen, Burlington, Canada). The Lipid reagent and Bacmid DNA were diluted separately into 100 μ l of Grace's medium without antibiotics, and combined to form lipid-DNA complexes and incubated at 22°C for 45 min. Medium from Sf9 was removed and cells were washed with 2 ml of Grace's medium (Invitrogen, Burlington, Canada). The lipid-DNA complexes were then diluted to 1 ml with Grace's medium, laid over the washed Sf9 cells and incubated at 28°C for 5 h. The medium was then removed and cells were incubated for another 72 h in 2 ml of SF-900 II SFM medium containing antibiotics. Medium was collected and clarified by centrifugation at 500 g's for 5 min. Recombinant baculovirus were harvested from supernatant and amplified by subsequent infection steps in Sf9 cells as described in the pFastBac Kit protocol (Invitrogen, Burlington, Canada).

Titration of Recombinant Baculovirus by Expression in Sf9 Cells

In order to maximize the expression level of hNPRA-ECD's in Sf9 cells, we tested the MOI ratio of recombinant baculovirus over Sf9 cells by sequential dilution. Briefly, Sf9 cells (5×10^5) were incubated in 50 ml SF-900 II SFM medium in 250 ml Erlenmeyer Flasks on a rotating

shaker for 48 h at 28°C. At the end of the incubation, 2 µg of Leupeptin and Aprotinin were added, followed by increasing amounts of recombinant baculovirus and the incubation was prolonged for another 72 h. A cocktail of proteases inhibitors (2 µg/ml Aprotinin, 2 µg/ml Leupeptin, 2 µg/ml Pepstatin, 0.2 mg/ml Pefabloc and 0.1 mM EDTA) was then added and Sf9 cells were centrifuged at 500 g for 5 min at 4°C. The supernatants were collected and an aliquot were denatured in Laemmli sample buffer and submitted to electrophoresis as described below. After the Western blot (see below), bands corresponding to the protein of interest were evaluated by densitometry. The baculovirus dilution corresponding to the maximum level of expression was used to scale up the production of hNPRA-ECD.

Expression of hNPRA-ECD^{WT} and hNPRA-ECD^{C423S} Mutant in Sf9 Cells

Sf9 cells (5×10^8) were incubated in 1000 ml of SF-900 II SFM medium in 250 ml Erlenmeyer flasks (100 ml/flask) on a rotating shaker for 48 h at 28°C. Typically, 4 ml of recombinant baculovirus was added and the incubation was prolonged for another 72 h in the presence of Leupeptin and Aprotinin. After the addition of the protease inhibitors cocktail, the mediums containing the ECD^{WT} and the ECD^{C423S} were clarified by centrifugation at 500 g for 5 min at 4°C and purified to homogeneity.

Purification of hNPRA-ECD

The hNPRA-ECD^{WT} and the hNPRA-ECD^{C423S} were dialysed against 20 volumes of buffer containing 30 mM Tris-HCl pH 7.4, 0.1 mM EDTA and loaded on a 50 ml bed of anionic exchanger QMA (Waters, Mississauga, Canada) equilibrated with the dialysing buffer. The gel was then washed with 5 volumes of 5 mM NaPO₄ pH 7.4, 30 mM NaCl, 0.1 mM EDTA and

proteins were eluted with 250 ml of 50 mM NaPO₄ pH 7.4, 300 mM NaCl, 0.1 mM EDTA. After addition of 15% glycerol and 10 mM imidazole, the eluate was loaded on a 3 mL Ni-NTA column (Qiagen, Mississauga, Canada). The gel was washed with 30 mL of 50 mM NaPO₄ pH 7.4, 300 mM NaCl, 0.1 mM EDTA and proteins were eluted with 6 mL of the same buffer containing 300 mM imidazole.

The purified ECD was then loaded on 1 ml ANP-agarose affinity column and washed with 50 mM NaPO₄ pH 7.4, 300 mM NaCl, 0.1 mM EDTA. The pure protein was eluted with 5 volumes of 1 ml of 50 mM Sodium Acetate pH5.0, 1M NaCl, 0.1 mM EDTA in tubes containing 12 ul of 1 M Sodium-HEPES in order to neutralize the pH. The high degree of purity of the hNPRA-ECD was confirmed by Coomassie staining of proteins after analytical SDS-PAGE under reducing and non-reducing conditions.

Electrophoresis and Immunoblot Analysis

For the electrophoresis, proteins were solubilized in Laemmli sample buffer (62 mM Tris-HCl, 2 % SDS, 10 % glycerol, 0.001 % Bromophenol blue, pH 6.8) and heated at 100°C for 3 min. For the reducing condition, 5 % β-mercaptoethanol was added to the sample buffer prior to boiling. Electrophoresis was performed in 7.5 % polyacrylamide gel. Proteins were stained in protein staining solution PageBlue (Fermentas, Burlington, Canada) as specified by the manufacturer. For the Western blot, proteins were electrotransferred from polyacrylamide gel to a nitrocellulose membrane (Bio-Rad, Mississauga, Canada) using the liquid Mini Trans-Blot (Bio-Rad, Mississauga, Canada). Detection of hNPRA-ECD was achieved using a Tetra-His Antibody (Qiagen, Mississauga, Canada) and the specific signal was probed with a horseradish peroxidase-coupled secondary antibody, according to the ECL Western blotting analysis system (GE

Healthcare, Mississauga, Canada). Under reducing conditions, hNPRA-ECD^{WT} behaves as a 56 kDa protein while hNPRA-ECD^{C423S} showed an apparent molecular weight of 109 kDa and 56 kDa under non-reducing and reducing conditions, respectively.

Radioligand Binding Assays

Competitive binding assays were performed in 200 μ l of 50 mM NaPO₄ pH 7.4, 100 mM NaCl, 0.1 mM EDTA, 0.05% Lysozyme, 0.1% BSA containing 67 fmoles (200,000 CPM) and 13 fmoles (40,000 CPM) of [¹²⁵I]ANP for incubation with the ECD^{WT} and the ECD^{C423S} respectively. Increasing concentrations of indicated competing peptides were added and the reaction was initiated by the addition of 7.4 ng (132 fmoles of monomer) for the ECD^{WT} and 4.3 ng (39 fmoles of dimer) for the ECD^{C423S}. After 22 hours at 22°C, the tubes were cooled down at 4°C. 100 μ l of the reaction medium was loaded on 1.8 ml Sephadex G-50 (GE Healthcare, Mississauga, Canada) and eluted with 50 mM NaPO₄ pH 7.4, 100 mM NaCl, 0.1 mM EDTA. The void volume containing the ECD-bound radioligand was recovered and quantified in a PerkinElmer gamma counter (PerkinElmer, Waltham, MA).

Kinetic assays were performed under the same conditions as the binding assays. Association was initiated by the addition of [¹²⁵I]ANP (0.3 nM and 66 pM, for ECD^{WT} and ECD^{C423S}, respectively). Dissociation was initiated by the addition of an excess of unlabeled rANP (1 μ M). The amount of specific binding was assessed at different times of incubation at 22°C, as described above.

Labeling of Mutant at the Cys⁴³² with Fluorescent Probe

The residue Cys⁴³², which is involved in the interchain disulfide bridge of homodimeric hNPRA-ECD^{C423S}, was used as specific site for anchoring fluorescent probes. In order to expose free Cys⁴²³, 125 µg of pure hNPRA-ECD^{C423S} was reduced in 250 µl of 50 mM HEPES pH 7.4, 0.1 mM EDTA by reacting at room temperature for 10 min with 20 µl of 80 mM TCEP (Promega Biosciences, San Luis Obispo, CA) in HEPES buffer. After the addition of 12.5 µl DMSO containing 250 µg Alexa Fluor 488 C5 maleimide (Invitrogen, Burlington, Canada), the reaction was carried for two additional hours at room temperature, followed by an overnight incubation at 4⁰C. The labeled protein was separated from unreacted fluorophore by gel permeation chromatography on PD-10 column (GE Healthcare, Mississauga, Canada) using 50 mM NaPO₄ pH 7.4, 100 mM NaCl, 0.1 mM EDTA as eluant. The final cleaning of the hNPRA-ECD-AF488 labelled protein was achieved by chromatography on Ni-NTA column as described above. The protein was aliquoted and kept frozen at –80⁰C in 10 % glycerol until used.

Measurement of ECD dimerization by FRET Homotransfer

17.6 ng (332 fmoles of monomer) of hNPRA-ECD-AF488 was pre-incubated in 100 µl of 50 mM NaPO₄ pH 7.4, 100 mM NaCl, 0.1 mM EDTA, 0.05% Lysozyme, 0.1% BSA, Tween 0.01% for 60 min at 22⁰C in black untreated 96-well (Corning, New-York, NY). 100 µl of increasing concentrations of indicated peptides were then added and the plates were placed on a rotating shaker for 20 sec and incubated at 22⁰C for another hour in the dark. The fluorescence was then measured for 5 sec, using a Victor 2 Multi-label Counter (PerkinElmer, Waltham, MA) with the excitation filter set at 485 nm. The fluorescence was recorded at 535 nm for 5 sec. Net

fluorescence was corrected by subtraction of background values measured in the absence of ECD protein.

Molecular modelling of NP-hNPRA-ECD

All calculations were performed using the software package SYBYL (Tripos, St. Louis, MO). The Tripos force field was used for energy calculations and a dielectric constant of 1 was used. The X-ray crystal structure of rANP 7-27 bound to the rat NPRA dimer (Hogawa et al., 2004) was used as a template for the receptor-bound form of hNPRA-ECD. Each variable amino acid within the ECD dimer complex was replaced one at a time by its equivalent in hNPRA sequence. The backbone dihedral angles were held fixed to preserve the receptor's secondary structure, while the amino acid side chains were positioned using the scan subroutine in SYBYL. This routine rotates each side chain dihedral angle until a sterically acceptable conformation was obtained. The complex was then energy minimized for 1,000 steps. No major conformational changes were observed during the minimization process. Modeling of the superagonist BANP bound to hNPRA was based on the contact points found using the photoaffinity results previously reported (Jossart et al. 2005). Both backbone and side chain dihedral angles of these residues were manipulated until steric complementarity with the receptor dimer was obtained and the required ligand to receptor contact was formed. At this point the complex was again subjected to 1000 steps of minimization. For modeling of the antagonist A71915 bound to hNPRA, the NPRA-bound structure of rANP 7-27 reported (Hogawa et al., 2004) was properly modified by deletion and substitution to yield the shorter 11 residue disulfide-bridged loop. Conserved residues between A71915 and rANP 7-27 were then placed at equivalent positions in

the binding cleft of the receptor dimer. The complex was then adjusted for steric complementarities with the receptor, and subjected to 1000 steps of minimization.

Data Analysis and Statistics

Dose-response curves for were analyzed by nonlinear least squares regression using the four-parameter logistic equation (De Léan et al., 1978):

$$Y = D + \frac{A - D}{1 + \left(\frac{X}{C}\right)^B} \quad (1)$$

where X is the concentration of agent, Y is the response measurement, A is the basal response value in the absence of agent, D is the maximal response value at high concentration of agent. B is the slope factor of the curve and C is the concentration of agent at 50% response level.

Radioligand binding saturation and competition curves were analyzed by nonlinear least squares regression using a model based on the law of mass action for the binding of two ligands to a single class of receptor sites (De Léan et al., 1982). Radioligand binding association kinetics data were analyzed using a model for second order ligand binding to a single class of sites (Rodbard 1973):

$$B = \frac{V \cdot (U - B_0) - U \cdot (V - B_0) \cdot e^{-k_{on} \cdot (U - V) \cdot t}}{(U - B_0) - (V - B_0) \cdot e^{-k_{on} \cdot (U - V) \cdot t}} \quad (2a)$$

where

$$U = \frac{(k_{on} \cdot L_t + k_{on} \cdot R_t + k_{off}) + \sqrt{(k_{on} \cdot L_t + k_{on} \cdot R_t + k_{off})^2 - 4 \cdot k_{on}^2 \cdot L_t \cdot R_t}}{2k_{on}} \quad (2b)$$

$$V = \frac{(k_{on} \cdot L_t + k_{on} \cdot R_t + k_{off}) - \sqrt{(k_{on} \cdot L_t + k_{on} \cdot R_t + k_{off})^2 - 4 * k_{on}^2 \cdot L_t \cdot R_t}}{2k_{on}} \quad (2c)$$

B_0 equals initial binding at time zero of association kinetics, k_{on} and k_{off} as association and dissociation constants, respectively, and t is time since beginning of association kinetics.

Dissociation kinetics data were analyzed using a model for a single exponential component:

$$B = B_0 \cdot e^{-k_{off} \cdot t} \quad (3)$$

Statistical testing of repeat experiments was performed by ANOVA, followed by posthoc Dunnett's or Student-Newman-Keuls test. The logarithmic transform of IC_{50} s were used for statistical tests in the case of competition binding and fluorescence quenching studies.

Results

Characterization of Soluble hNPRA-ECD WT and C423S Mutant

Expression of the rat extracellular domain of NPRA in mammalian cell lines has been previously described (Labrecque et al., 1999; Misono et al., 1999). Based on size-exclusion chromatography, the rat NPRA-ECD behaved in solution as a monomer in the absence of ANP and as a dimer in the presence of ANP (Misono et al., 1999). Expression of human NPRA-ECD in HEK-293 cells proved to be more difficult and produced a low yield (data not shown). We therefore expressed the human ECD in Sf9 cells, following replacement of the original signal peptide sequence by that of melittin and by addition of a carboxy-terminal hexahistidine tag. The secreted ECD was harvested in the Sf9 cell culture medium and purified by metal-chelate and affinity chromatography. The pure ECD monomer was obtained at a decent level (100 µg/L). Microsequencing of the amino-terminal of the ECD documented the expected sequence of the mature form (GNLT(V)AVVLP...), confirming that cleavage of the melittin signal peptide was properly processed in SF9 cells. The protein displayed a single homogeneous band of 56 kDa on PAGE (Figure 1), suggesting that the protein core (~50 kDa) was glycosylated in this expression system. Detection of Asn² by microsequencing confirmed however that this residue was not glycosylated.

We have formerly documented that mutation C423S of rat NPRA disrupts a short disulfide-bridged decapeptide and exposes an unpaired Cys⁴³² which covalently dimerizes NPRA in a fashion reminiscent of that of clearance-type receptor NPRC (Labrecque et al., 1999). This mutation also constitutively activates NPRA. It also provides a covalent dimeric form of the soluble NPRA-ECD with an affinity for ANP which is similar to that of full length NPRA

(Labrecque et al. 1999). This mutation was applied to human NPRA-ECD. It yielded a homogeneous 106 kDa band on non-reducing PAGE (Figure 1), with very little monomeric form. hNPRA-ECD^{C423S} was more easily purified and was more avidly retained on ANP affinity gel than NPRA-ECD^{WT}, presumably because of its covalently dimeric state and its higher affinity for ANP.

Equilibrium Binding and Kinetics of ANP on NPRA-ECD WT and C423S Mutant

Soluble hNPRA-ECD^{WT} proved to be fully competent under equilibrium binding conditions, with a dissociation constant (K_d) of 7.9×10^{-10} M for ANP (Table 1). As expected for a soluble monomeric ECD, this affinity is somewhat lower than that documented for membrane hNPRA (K_d 1.3×10^{-10} M, Bodart et al., 1996) or intact cell receptor (K_d 1.6×10^{-10} M, Jewett et al., 1993). In contrast, the disulfide-bridged hNPRA-ECD^{C423S} displayed a significantly higher affinity (K_d 1.3×10^{-10} M, $p < 0.01$, Table 1) than that for the WT form. This higher affinity of the C423S mutant matched that for the membrane receptor, again strongly suggesting that functional NPRA is naturely dimeric (Labrecque et al., 1999).

For cytokine homodimeric receptors, such as GHR, and heterodimeric receptors, such as IFNAR, ligand binding proceeds sequentially in two steps. Cytokines interact with one receptor subunit of the ECD. Then, dimerization of the ECD increases affinity for the ligand by slowing down the rate constant of dissociation (k_{off}) of the cytokine (Cunningham et al., 1991; Lamken et al., 2004). In order to test whether this mechanism applies to homodimeric NPRA, we compared the association and dissociation kinetics of ANP to NPRA-ECD WT and C423S mutant (Figure 2 and Table 1). Binding of ANP to the ECD^{WT} was characterized by an overall k_{on} of 4×10^5 M⁻¹s⁻¹, typical of protein-protein interactions (Schlosshauer and Baker, 2007). However the association

kinetics displayed a slight deviation from a second order reaction and could be compatible with a two-step process. This suggested that a rate-limiting step was involved, which might correspond to dimerization of the ECD monomers. The dissociation kinetics of ANP from the ECD-WT was very slow and monophasic, with a single k_{off} of $7.6 \times 10^{-5} \text{ s}^{-1}$. In the case of the covalently dimeric ECD^{C423S} mutant, association kinetics of ANP was monophasic, with a 16-fold faster k_{on} of $6.6 \times 10^6 \text{ M}^{-1} \text{ s}^{-1}$, strongly suggesting that the rate-limiting step required for dimerization of the ECD was absent for this mutant. However, the dissociation rate constant k_{off} of $8.4 \times 10^{-5} \text{ s}^{-1}$ was very similar to that for the ECD^{WT}. These results contrast with those obtained for cytokine receptors and indicate that a different mechanism most probably occurs for NPRA. A plausible scheme would involve the binding of ANP to preformed ECD dimers. Kinetically derived estimates of dissociation constants (K_d), calculated as the ratio $k_{\text{off}}/k_{\text{on}}$, deviate from estimates obtained with equilibrium binding results (Table 1). Such a discrepancy is not uncommon and suggests that a more complex binding process is occurring for the ECD^{WT} and ECD^{C423S} mutant, possibly involving fast rebinding of ANP while still in its active conformation.

Specificity of Binding for Natriuretic Peptide Agonists and Antagonist

In contrast with rNPRA, hNPRA is highly selective for full length ANP 1-28 (Schoenfeld et al., 1995). hANP and rANP have nearly identical potencies on hNPRA. However hANP contains a unique residue Met¹² which is oxidized under experimental conditions, leading to a potency loss. Therefore, rANP was preferred as a reference ligand. hBNP is ~8-fold less potent than ANP, and even ~2-fold weaker than pBNP32. CNP, the NPRB-selective peptide, is inactive at submicromolar concentrations. In order to check whether the soluble hNPRA-ECD could maintain the peptide binding properties of membrane receptor, we tested the specificity of soluble hNPRA-ECD, using a series of natural natriuretic peptides and analogs with agonist and

antagonist properties (Table 2 and Figure 3). rANP was ~10-fold more potent than pBNP32, while CNP, which is specific for NPRB, and C-ANF, which is specific for NPRC, were inactive.

Interestingly, BANP, which is a chimeric peptide with the cyclic portion from pBNP32 and the exocyclic segments from ANP, proved to be 13-fold more potent than the natural ligand ANP. This confirms the unique properties of this superagonist that we have previously reported (Mimeault et al., 1993; Bodart et al., 1996). Testing of the kinetics of BANP binding to hNPRA-ECD^{WT} indicated that the higher affinity of the superagonist is due to both a 10-fold faster k_{on} ($7.4 \pm 1.6 \times 10^6 \text{ M}^{-1} \text{ s}^{-1}$, data not shown) and a slower k_{off} ($< 10^{-5} \text{ s}^{-1}$, data not shown), when compared with rANP (Table 1). The size-reduced miniANP (Li et al., 1995) proved to be ~9-fold less potent than ANP. In addition, we tested the potency of the small peptide antagonist A71915 (von Geldern et al., 1990) in this system. A71915 displayed micromolar affinity and completely inhibited ANP binding at 10 μM (Figure 3 and Table 2). The potency order BANP>ANP>BNP~mini-ANP>>A71915>>CNP~C-ANF confirms that the ECD provides a reliable model for the peptide binding site of hNPRA.

Dimerization of ECD^{WT}

We have previously shown (Rondeau et al., 1995) that ANP is binding to NPRA homodimeric subunits in a 1:2 stoichiometric ratio and that a single peptide is contacting both monomers. This was later confirmed by crystal structure determination (Ogawa et al., 2004). Misono et al have documented by size-exclusion chromatography that soluble rat NPRA-ECD behaved as monomer in the ligand-free state, but as a homodimer when bound to ANP (Misono et al., 1999). However the ligand specificity of the dimerization process was not established. We therefore established a homogeneous assay for soluble hNPRA-ECD which enables measurement in solution of the dimerization state without phase separation. Covalently dimeric hNPRA-

ECD^{C423S} was monomerized by reduction with CTEP and derivatized on free Cys⁴³² with Alexa Fluor 488-maleimide. The residue Cys⁴³² is normally located in a decapeptide disulfide-bridged loop under the membrane-proximal lobe of the ECD. Mutation C423S disrupts the loop, resulting in a flexible region with poorly defined secondary structure and leaving Cys⁴³² exposed and reactive. The resulting fluorescent ECD monomer behaved in ANP binding assays with the same affinity as for underivatized hNPRA-ECD^{WT} (data not shown). Ligand-induced dimerization of the derivatized ECD is expected to bring the two fluorophores of the subunits close together (< 50Å). At this short distance, fluorescence resonance energy homotransfer (autoquenching) should reduce overall fluorescence (Tricerri et al., 2001). As shown in Figure 4, addition of ANP significantly inhibited fluorescence, directly documenting in solution ligand-induced dimerization without any perturbation by a separation step. The addition of as small as a 1.4-fold excess of underivatized monomeric ECD^{WT} drastically reduced the proportion of fluorescent ECD homodimer to 18% of control (Figure 4). Addition of ECD^{WT} lead to an almost complete reversal of fluorescence autoquenching induced by ANP. Addition of ECD^{WT} in the absence of ANP also slightly but significantly increased fluorescence (Figure 4). This strongly suggests that a small portion of ECD is spontaneously dimeric even in the absence of ANP. Attempts to document ANP-induced dimerization of hNPRA-ECD by FRET heterotransfer using Alexa Fluor 350 and Alexa Fluor 488 as the donor-acceptor pair confirmed those results (data not shown). However, this heterotransfer system was much less sensitive than with homotransfer and required at least 20-fold higher concentrations of derivatized-ECD. Autoquenching based on Alexa Fluor 488-derivatized ECD was therefore used for subsequent studies.

Since agonists are expected to bind to hNPRA-ECD as a homodimeric receptor, we then tested the specificity of natriuretic peptides and analogs in inducing autoquenching observed with ANP. As shown in Figure 5 and Table 2, agonists dose-dependently inhibited fluorescence with a potency order BANP>ANP>BNP>mini-ANP. Potency estimates of peptides on fluorescence quenching was highly correlated ($r=0.99$, $p<0.002$) with those for ANP binding competition when expressed on a logarithmic scale (Table 2), indicating that high affinity binding involves the dimeric state of hNPRA-ECD. The NPRB-selective peptide CNP was inactive, even at micromolar concentrations. Interestingly, the antagonist A71915 also inhibited fluorescence, indicating that the antagonist is binding to a homodimeric form of hNPRA-ECD. This contrasts with the results obtained for GH antagonists, which bind to GHR monomer and which fail to induce receptor dimerization (Cunningham et al, 1991; Cunningham and Wells, 1993). In addition, dose-response curves for autoquenching all displayed a lower plateau at high peptide concentration (Figure 5), indicating that excess peptide could not lead to receptor ECD monomerization. This is again in contrast with GHR (Cunningham et al., 1991), for which GH favors receptor dimerization only at low concentration. This would be expected for such a system where the agonist first binds with high affinity to an ECD monomer, followed by ECD dimerization which further increases the affinity for the agonist. The absence for ANP and analogs of any high concentration reversal of dimerization strongly argues that natriuretic peptides, agonists or antagonists, essentially bind to preformed dimeric ECD.

The maximum level of autoquenching obtained at high concentration of peptides was quite reproducible for each peptide, but clearly differed among them (Table 2). The maximal quenching for the agonist pBNP32 and the antagonist A71915 highly significantly differed from

that of ANP and BANP. The higher quenching observed is consistent with a smaller distance between the ECD subunits (Tricerri et al., 2001). Thus, while all peptides bind to a dimeric form of the ECD, the conformation of the ECD dimer appears to differ among agonists and especially between the agonists and the antagonist.

Molecular Modeling of NP-NPRA-ECD Complex

The crystal structure of rNPRA-ECD bound to rANP 7-27 has been reported (Ogawa et al., 2004). The truncated peptide used, equivalent to Atriopeptin II, lacks the exocyclic amino-terminal and the carboxy-terminal residue Tyr²⁸. It displays low potency, especially on hNPRA (Schoenfeld et al., 1995). Nevertheless, it exemplifies the flat conformation of the natriuretic peptide ring, which is tightly bound in the cleft between the ECD subunits. Since hNPRA and rNPRA sequences mostly differ in their ECD portion and since their affinities for natriuretic peptides are also divergent (Schoenfeld et al., 1995), it was necessary to derive a structural model for the hNPRA ECD and to compare it to that for rNPRA ECD. Such a model is expected to document the interactions between the peptides and the receptor subunits. It might explain the higher affinity of the superagonist BANP relative to ANP. The model could also document the peculiar positioning of the antagonist A71915 within the peptide binding cleft. All residues of the ECD which differ between hNPRA and rNPRA were properly substituted and the resulting model, bound to ANP 7-27, was energy-minimized (Figure 6A and Table 3). The peptide was then replaced by a previously documented conformation of the superagonist BANP (Jossart et al., 2005), or by modifying ANP into the antagonist A71915 (Figure 6B and C, Table 3). Two outstanding regions of the ligand binding interface of natriuretic peptide receptors involve hydrophobic regions (He et al., 2006). Hydrophobic pocket 1 of chain A binds Phe⁸ of ANP or BANP, and Cha⁸ of A71915 and the residues involved are highly conserved (Figure 6, Table 3).

Hydrophobic pocket 2 of chain B binds Gln¹⁸ of ANP or Leu¹⁸ of BANP, while the non-natural residue D-Tic¹⁶ of A71915 interacts with the margin of pocket 2. BANP contains an excess of positive charges provided by the amino terminal and six arginines. Correspondingly, a number of acidic residues are located on the surface of the peptide binding cleft. Both the amino-terminal and Arg³ of BANP interact with Asp¹⁷⁷ of chain A. Arg⁴ is located close to Asp¹⁹² of subunit B, Arg¹¹ is in contact with Glu¹⁸⁷ of chain B, Arg¹⁴ is close to Asp⁶² of chain B, while Arg²⁷ is interacting with Glu¹⁸⁷ of subunit A (Table 3). The carboxy-terminal residue Tyr²⁸ of BANP is located in the vicinity of Met¹⁷³ and is facing the opposite edge of the binding cleft (Figure 6B). This contrasts with the positioning of the carboxy-terminal residues of the truncated ANP 7-27 which binds over and occupies the position of the amino-terminal portion of full length natriuretic peptide (Figure 6A, Table 3). This suggests that the expected conformation of the exocyclic portions of native ANP 1-28, which includes both amino- and carboxy-terminal segments, is more accurately represented by the complex obtained with BANP (Figure 6B). This is in agreement with previous observations on the contribution of both the amino- and the carboxy-terminal to the potency of ANP on human NPRA (Schoenfeld et al., 1995). Several residues of the cyclic portion of BANP (Arg¹¹, Leu¹², Ile¹⁵, Ser¹⁷) interact with different residues of the receptor than those for ANP 7-27 (Table 3). This might contribute to the higher affinity and potency of BANP relative to ANP, since the ring portion of the natriuretic peptides is central to their tight interaction with NPRA.

Docking of the antagonist A71915 indicates that, despite the fact that this antagonist is about half the size of full length agonists such as ANP or BANP, a single molecule of the ligand could fit in the binding cleft (Figure 6C). Interestingly, the interactions of the crucial residues

FGGRFRI of the ring portion seem to be conserved for A71915. However residue D-Tic¹⁶ appears to constraint binding of the peptide and to result in a suboptimal fitting with hydrophobic pocket 2. This might possibly explain the antagonistic character of A71915. It is also likely associated with the closer dimer conformation documented by FRET autoquenching (Figure 5 and Table 2).

Discussion

We have shown that natriuretic peptide binding to NPRA does not conform to the cytokine receptor model exemplified by GHR. In contrast to cytokines which present a well defined secondary structure both in the free and the receptor-bound states, natriuretic peptide conformation is disordered in solution (Carpenter et al., 1997). When binding to NPRA, the peptides must acquire a flat penny-like conformation by selection or induction. Perhaps due to their stable conformation in solution, cytokines first bind with nanomolar affinity to one receptor subunit. Interaction with the second receptor subunit then stabilizes the high affinity dimer, resulting in a slower dissociation rate. At higher concentration however, two molecules of cytokines can bind their homodimeric receptor, resulting in its monomerization and in loss of activation. Again in contrast with cytokines, natriuretic peptides appear to bind only to a preformed dimeric state of NPRA. This is documented by the flat high-dose asymptote of the homo-quenching dose-response curve which occurs for all peptides (Figure 3), contrasting with GHR (Cunnhingham, et al., 1991).

Slower and apparently more complex association kinetics of ANP to soluble ECD^{WT} than to covalently dimeric ECD^{C423S} indicates that spontaneous dimerization constitutes the rate limiting step of the ligand binding process (Figure 7). In contrast with the conclusions of a previous report (Misono et al., 1999), it is proposed that ECD^{WT} dimers are present in solution at submicromolar concentration. However, the fast monomerization constant (k_{mon}) would preclude the documentation of spontaneous dimers in assay systems involving phase separation such as size exclusion chromatography. The use of a homogeneous assay involving FRET homoquenching provided the first evidence for spontaneous dimer formation at nanomolar concentration of ECD

(Figure 4). Further documentation of the kinetic properties of the dimerization and the ligand binding steps will be required in order to completely characterize this proposed mechanism (Figure 7). Binding of natriuretic peptides to NPRA-ECD is quite stable (Figure 1, Table 1). The affinity of ANP for the covalently dimeric soluble ECD^{C423S} closely mimics that observed with full length cellular NPRA. This agrees with previous results obtained with rNPRA-ECD (Labrecque et al., 1999), and with previous observations that full length NPRA is spontaneously homodimeric.

The correlation of the rank order of potency for natriuretic peptides in ligand binding (Figure 3) and ECD dimerization assays (Figure 4, Table 2) again confirms that all natriuretic peptides bind to the dimeric state of the ECD. The lower potency of the antagonist A71915 could be interpreted as due to its smaller size (13 vs 28 residues for ANP). However, the agonist mini-ANP (15 residues) still conserves high affinity, albeit reduced relative to that for full length ANP. Thus the lower affinity of A71915 might be due to its altered conformation. For erythropoietin receptor, both agonists and antagonists also bind to the dimeric form of the receptor (Syed et al., 1998). However, the conformation of the receptor dimer differs between various ligands. Our results on distinct maxima of fluorescence auto-quenching (Figure 5 and Table 2) also show that the conformation of the ligand-bound NPRA-ECD dimer differs among peptides. The antagonist A71915 mostly differs from the results for ANP (Table 2). This would be compatible with a shorter distance between the fluorophores located in the carboxy-terminal region of the ECD. This might be associated with an axial or a lateral rotation of the ECD subunits, leading to an inactive conformation of the receptor. The constrained interaction of residue D-Tic¹⁶ of A71915 with hydrophobic pocket 2 of the ECD is potentially associated with the antagonistic properties.

Indeed, substitution in A71915 of D-Tic¹⁶ with the natural residue L-Phe¹⁶ leads to the full agonist A68828 (von Geldern et al., 1992).

The conformational change occurring during activation of NPRA is still unknown. Agonist binding to the homodimeric ECD appears to alter the positioning of the receptor subunits, possibly according to a rotation mechanism (Ogawa et al., 2004). This was predictable based upon previous results using cysteine substitution of the extracellular juxtamembrane domain. Mutation C423S of NPRA, leading to an unpaired Cys⁴³², results in spontaneous disulfide bridge formation, indicating that the juxtamembrane regions of the ECD subunits should be juxtaposed (Labrecque et al., 1999). However mutation D435C, producing an unpaired Cys⁴³⁵ three residues distal to Cys⁴³², leads to a disulfide bridge only upon NPRA activation by ANP (Labrecque et al., 2001). These results are compatible with a conformational change of the juxtamembrane domain which was also documented in the present work by FRET auto-quenching. Whether this change is due to an axial rotation or to a lateral movement of the subunits is not yet clear. For cytokine receptors, one prevalently proposed activation mechanism involves subunit rotation within a receptor dimer (Brown et al, 2005). The structure of the juxtamembrane region of NPRA-ECD is not well documented in the reported crystallographic studies of soluble ECD. The proper conformation of this region is most probably dependent on its natural proximity to the plasma membrane and should ultimately be studied in the presence of a phospholipid bilayer. Further studies will be required for documenting this activation conformational change of NPRA. The homogenous FRET assay described in this study provides a new experimental approach for detailing the kinetic steps involved in natriuretic peptide receptor binding and activation. Its high sensitivity and accuracy could also prove valuable in the study of agonist- and antagonist-specific conformations of the receptor.

Acknowledgments

We thank Claude Lazure from Clinical Research Institute of Montreal for micro-sequencing the purified hNPRA-ECD.

References

- Bodart V, Rainey WE, Fournier A, Ong H, De Lean A (1996) The H295R human adrenocortical cell line contains functional atrial natriuretic peptide receptors that inhibit aldosterone biosynthesis. *Mol Cell Endocrinol* **118**:137-144.
- Brown RJ, Adams JJ, Pelekanos RA, Wan Y, McKinsty WJ, Palethorpe K, Seeber RM, Monks TA, Eidne KA, Parker MW, Waters MJ (2005) Model for growth hormone receptor activation based on subunit rotation within a receptor dimer. *Nat Struct Mol Biol* **12**:814-821.
- Carpenter KA, Wilkes BC, De Lean A, Fournier A, Schiller PW (1997) Hydrophobic forces are responsible for the folding of a highly potent natriuretic peptide analogue at a membrane mimetic surface: an NMR study. *Biopolymers* **42**:37-48.
- Cunningham BC, Ultsch M, de Vos AM, Mulkerrin MG, Clauser KR, and Wells JA (1991) Dimerization of the extracellular domain of the human growth hormone receptor by a single hormone molecule. *Science* **254**:821-825.
- Cunningham BC, and Wells JA (1993) Comparison of a structural and a functional epitope. *J Mol Biol* **234**:554-563.
- De Léan A, Munson PJ, and Rodbard D (1978) Simultaneous analysis of families of sigmoidal curves: application to bioassay, radioligand assay, and physiological dose-response curves. *Am J Physiol* **235**:E97-E102.

De Léan A, Hancock AA, and Lefkowitz RJ (1982) Validation and statistical analysis of a computer modeling method for quantitative analysis of radioligand binding data for mixtures of pharmacological receptor subtypes. *Mol Pharmacol* **21**:5-16.

de Vos AM, Ultsch M, Kossiakoff AA (1992) Human growth hormone and extracellular domain of its receptor: crystal structure of the complex. *Science* **255**:306-312.

Duda T, Venkataraman V, Ravichandran S, Sharma RK (2004) ATP-regulated module (ARM) of the atrial natriuretic factor receptor guanylate cyclase. *Peptides* **26**:969-984.

Fuh G, Cunningham BC, Fukunaga R, Nagata S, Goeddel DV, Wells JA (1992) Rational design of potent antagonists to the human growth hormone receptor. *Science* **256**:1677-1680.

Gardner DG, Chen S, Glenn DJ, and Grigby CL (2007) Molecular biology of the natriuretic peptide system: implication for physiology and hypertension. *Hypertension* **49**:419-426.

He Xl, Chow Dc, Martick MM, Garcia KC (2001) Allosteric activation of a spring-loaded natriuretic peptide receptor dimer by hormone. *Science* **293**:1657-1662.

He XL, Dukkipati A, and Garcia KC (2006) Structural Determinants of Natriuretic Peptide Receptor Specificity and Degeneracy. *J Mol Biol* **361**: 698–714.

Jewett JRS, Koller KJ, Goeddel DV, and Lowe DG (1993) Hormonal induction of low affinity receptor guanylyl cyclase. *EMBO (Eur Mol Biol Organ) J* **12**:769-777.

Kuhn M (2004) Molecular physiology of natriuretic peptide signalling. *Basic Res Cardiol* **99**:76-82.

Jossart C, Coupal M, McNicoll N, Fournier A, Wilkes BC, De Léan A. (2005) Photolabeling study of the ligand binding domain of natriuretic peptide receptor a: development of a model. *Biochemistry* **44**:2397-2408.

Joubert S, Labrecque J, De Lean A (2001) Reduced activity of the NPR-A kinase triggers dephosphorylation and homologous desensitization of the receptor. *Biochemistry* **40**:11096-11105.

Joubert S, Jossart C, McNicoll N, De Lean A (2005) Atrial natriuretic peptide-dependent photolabeling of a regulatory ATP-binding site on the natriuretic peptide receptor-A. *FEBS J* **272**:5572-5583.

Joubert S, McNicoll N, De Lean A (2007) Biochemical and pharmacological characterization of P-site inhibitors on homodimeric guanylyl cyclase domain from natriuretic peptide receptor-A. *Biochem Pharmacol* **73**:954-963.

Labrecque J, McNicoll N, Marquis M, and De Léan A (1999) A disulfide-bridged mutant of natriuretic peptide receptor-A displays constitutive activity - Role of receptor dimerization in signal transduction. *J Biol Chem* **274**:9752-9759.

Labrecque J, Deschenes J, McNicoll N, De Lean A (2001) Agonistic induction of a covalent dimer in a mutant of natriuretic peptide receptor-A documents a juxtamembrane interaction that accompanies receptor activation. *J Biol Chem* **276**:8064-8072.

Lamken P, Lata S, Gavutis M, and Piehler J (2004) Ligand-induced Assembling of the Type I Interferon Receptor on Supported Lipid Bilayers. *J Mol Biol* **341**:303-318.

Larose L, McNicoll N, Ong H, De Lean A (1991) Allosteric modulation by ATP of the bovine adrenal natriuretic factor R1 receptor functions. *Biochemistry* **30**:8990-8995.

Lee CY, Burnett JC Jr. (2007) Natriuretic peptides and therapeutic applications. *Heart Fail Rev* **12**:131-142.

Li B, Tom JY, Oare D, Yen R, Fairbrother WJ, Wells JA, Cunningham BC (1995) Minimization of a polypeptide hormone. *Science* **270**:1657-1659.

Mimeault M, Fournier A, Féthière J, De Léan A (1993) Development of natriuretic peptide analogs selective for the atrial natriuretic factor-R1A receptor subtype. *Mol Pharmacol* **43**:775-782.

Misono KS, Sivasubramanian N, Berkner K, and Zhang X (1999) Expression and Purification of the Extracellular Ligand-Binding Domain of the Atrial Natriuretic Peptide (ANP) Receptor: Monovalent Binding with ANP Induces 2:2 Complexes. *Biochemistry* **38**:516-523.

Ogawa H, Qiu Y, Ogata CM, and Misono KS (2004) Crystal Structure of Hormone-bound Atrial Natriuretic Peptide Receptor Extracellular Domain. *J Biol Chem* **279**: 28625–28631.

Padayatti PS, Pattanaik P, Ma X, van den Akker F (2004) Structural insights into the regulation and the activation mechanism of mammalian guanylyl cyclases. *Pharmacol Ther* **104**:83-99.

Potter LR, Abbey-Hosch S, Dickey DM (2006) Natriuretic peptides, their receptors, and cyclic guanosine monophosphate-dependent signaling functions. *Endocr Rev* **27**:47-72.

Rodbard D (1973) Mathematics of hormone-receptor interaction. I. Basic principles. *Adv Exp Med Biol* **36**:289-326.

Rondeau JJ, McNicoll N, Gagnon J, Bouchard N, Ong H, De Lean A (1995) Stoichiometry of the atrial natriuretic factor-R1 receptor complex in the bovine zona glomerulosa. *Biochemistry* **34**:2130-2136.

Rubattu S, Bigatti G, Evangelista A, Lanzani C, Stanzione R, Zagato L, Manunta P, Marchitti S, Venturelli V, Bianchi G, Volpe M, Stella P. (2006) Association of atrial natriuretic peptide and

type A natriuretic peptide receptor gene polymorphisms with left ventricular mass in human essential hypertension. *J Am Coll Cardiol* **48**:499-505.

Schlosshauer M and Baker D (2007) Realistic protein–protein association rates from a simple diffusional model neglecting long-range interactions, free energy barriers, and landscape ruggedness. *Protein Sci* **13**:1660-1669.

Schoenfeld JR, Sehl P, Quan C, Burnier JP, Lowe DG (1995) Agonist selectivity for three species of natriuretic peptide receptor-A. *Mol Pharmacol* **47**:172-180.

Strain WD (2004) The use of recombinant human B-type natriuretic peptide (nesiritide) in the management of acute decompensated heart failure. *Int J Clin Pract* **58**:1081-1087.

Syed RS, Reid SW, Li C, Cheetham JC, Aoki KH, Liu B, Zhan H, Osslund TD, Chirino AJ, Zhang J, Finer-Moore J, Elliott S, Sitney K, Katz BA, Matthews DJ, Wendoloski JJ, Egrie J, Stroud RM (1998) Efficiency of signalling through cytokine receptors depends critically on receptor orientation. *Nature* **395**:511-516.

Tricerri MA, Behling AK, Sanchez SA, Bronsky J, and Jonas A (2001) Arrangement of apolipoprotein A-I in reconstituted high-density lipoprotein disks: an alternative model based on fluorescence resonance energy transfer experiments *Biochemistry* **40**:5065-5074.

von Geldern TW, Budzik GP, Dillon TP, Holleman WH, Holst MA, Kiso Y, Novosad EI, Opgenorth TJ, Rockway TW, Thomas AM and Yeh S (1990) Atrial natriuretic peptide antagonists: biological evaluation and structural correlations. *Mol Pharmacol* **38**:771-778.

von Geldern TW, Rockway TW, Davidsen SK, Budzik GP, Bush EN, Chu-Moyer MY, Devine EM Jr, Holleman WH, Johnson MC, Lucas SD, Pollock DM, Smital JM, Thomas AM, and Opgenorth TJ (1992) Small atrial natriuretic peptide analogues: design, synthesis, and structural requirements for guanylate cyclase activation. *J Med Chem* **35**:808-816.

Footnotes

This work was supported by grants from Canadian Institutes of Health Research and Groupe d'Étude des Protéines Membranaires of Fonds de Recherche en Santé du Québec.

Address correspondence to: André De Léan, Department of Pharmacology, Faculty of Medicine, Université de Montréal, 2900 boulevard Édouard-Montpetit, Pavillon Principal, V437-1, Montréal, Québec, Canada H3T 1J4. Email: delean@pharmco.umontreal.ca.

Legends for figures

Figure 1: Coomassie staining of purified hNPRA-ECD WT and C423S. Purified hNPRA-ECD (WT and C423S) were subjected to SDS PAGE on 7.5 % polyacrylamide gel under non reducing conditions and stained with Coomassie Blue, as described in Materials and Methods. The positions of monomers (M) and disulfide-linked dimers (D) are indicated.

Figure 2: Association (A) and dissociation (B) kinetics for ANP. Association was initiated by addition of [125 I]ANP (0.33 nM and 65 pM, respectively) to purified hNPRA-ECD^{WT} (0.66 nM of monomer, closed circles) or hNPRA-ECD^{C423S} (0.195 nM of dimer, open circles). Dissociation was initiated by adding an excess of unlabeled rANP (1 μ M). The amount of specific binding was assessed at different times of incubation at 22°C as described in Materials and Methods. ANP binding is expressed as a fraction of equilibrium binding. Each data point represents the mean \pm S.E. of duplicate determinations. The results are representative of at least three identical experiments. Association and dissociation kinetics curves were fitted using models described in Materials and Methods. Kinetic parameters are shown in table 1.

Figure 3: Competition curves for peptides. Purified hNPRA-ECD^{WT} (0.66 nM of monomer) was incubated with [125 I]ANP (0.33 nM) and varying concentrations of indicated competing unlabeled peptides for 22h at 22°C, as described under Materials and Methods. ANP binding is expressed as a fraction of initial binding B_0 in absence of competing peptides. Each data point represents the mean \pm S.E. of duplicate determinations. The results are representative of at least three identical experiments. The curves were analyzed by nonlinear least squares regression as described (De Léan et al., 1982). IC₅₀ values for these peptides are shown in table 2.

Figure 4: Inhibition of ANP-induced homo-FRET by addition of excess WT. hNPRA-ECD-AF-488 (1.66 nM of monomer) was incubated with or without ANP (1 μ M), in presence or in absence of an excess of hNPRA-ECD^{WT} (2.26 nM of monomer). The fluorescence was measured after 1h of incubation at 22°C as described in Materials and Methods. Values represent averages from three separate experiments, each assayed in quadruplicate. ** $p < 0.01$, significantly different from all other groups. ††= $p < 0.01$, significantly different from Control.

Figure 5: Dose-response curves of peptides on FRET homotransfer. Increasing concentrations of indicated peptides were added to hNPRA-ECD-AF-488 (1.66 nM of monomer) and fluorescence was measured after 1h of incubation at 22°C, as described in Experimental Procedure. Fluorescence is expressed as mean \pm SE of four determinations. The results are representative of at least three identical experiments. IC₅₀ and F/F₀ values for these peptides are shown in Table 2.

Figure 6: Model for binding of ANP (A), BANP (B) and A71915 (C) to hNPRA-ECD dimer. Modeling of hNPRA-ECD in complex with peptides was carried out as described under Materials and Methods using SYBYL software. hNPRA-ECD homodimer subunits are shown in ribbon model. Peptides are shown in sticks model. Residues of peptides interacting with hydrophobic pocket 1 (subunit A) and 2 (subunit B) of ECD dimer are indicated.

Figure 7: Schematic model for ANP binding to hNPRA-ECD homodimer. The subunits of the soluble extracellular domain are represented as two connected lobes (dark grey), with the

membrane distal lobes interfacing each other when in the peptide-bound state. The plasma membrane (not shown) is assumed to be located below the ECD. The peptide ligand is presented as a small ellipse (light grey). The fast rates for the monomerization of the ECD (k_{mon}) and the association (k_{on}) of the ligand to the preformed ECD dimer are represented as thick arrows. The slow rates for ECD dimer formation (k_{dim}) and peptide dissociation (k_{off}) are shown as thin arrows.

Tables

Table 1: Kinetic parameters of [¹²⁵I]ANP binding to hNPRA-ECD. Kinetic assays were performed as mentioned under Materials and Methods and Fig. 2 legend. Radioligand binding association and dissociation kinetics data were analyzed using models described in Materials and Methods. Values are mean ± S.E. of three to four separate experiments (indicated in parenthesis), with each measurement done in duplicate.

	hNPRA-ECD ^{WT}	hNPRA-ECD ^{C423S}
k_{on} (M⁻¹s⁻¹)	4.04±0.50x10⁵ (3)	6.57±0.15x10⁶ (3)^a
k_{off} (s⁻¹)	7.55±1.17x10⁻⁵ (3)	8.45±0.42x10⁻⁵ (3)
k_{off}/k_{on} (M)	1.90±0.32x10⁻¹⁰ (3)	1.29±0.04x10⁻¹¹ (3)^a
K_d (M)	7.92±0.79x10⁻¹⁰ (4)	1.31±0.14x10⁻¹⁰ (4)^a
^a p<0.01		

Table 2: IC₅₀ for competition curves and FRET homotransfer. IC₅₀ were determined by competition binding and FRET homotransfer, as described under Materials and Methods and Fig. 3 and Fig.5 legends. F and F₀ are the net fluorescence of the hNPRA-ECD-AF-488 homodimer in the presence of the highest concentration of peptide or in its absence, respectively. Values are mean ± S.E. of three to four separate experiments (indicated in parenthesis), with each measurement done in duplicate or quadruplicate, for binding and quenching respectively. There was a high correlation (r=0.99, p<0.002) between the log of IC₅₀ from binding assays and those from fluorescence quenching studies

Radioligand binding		Fluorescence quenching	
Peptides	IC ₅₀	IC ₅₀	F/F ₀
	(M)	(M)	(Maximum)
BANP	2.72 ± 0.13 x 10 ⁻¹⁰ (3)	4.27 ± 0.52 x10 ⁻¹⁰ (3)	0.77 ± 0.03 (3)
rANP 1-28	1.77 ± 0.18 x 10 ⁻⁹ (4)	3.10 ± 0.72 x10 ⁻⁹ (4)	0.80 ± 0.03 (4)
mini-ANP	1.52 ± 0.11 x 10 ⁻⁸ (3)	2.18 ± 0.32 x 10 ⁻⁸ (3)	0.75 ± 0.01 (3) ^a
pBNP32	1.64 ± 0.10 x 10 ⁻⁸ (3)	7.70 ± 0.39 x 10 ⁻⁹ (3)	0.66 ± 0.01 (3) ^b
A-71915	1.04 ± 0.14 x 10 ⁻⁶ (3)	6.10 ± 0.99 x10 ⁻⁷ (3)	0.60 ± 0.02 (3) ^b
C-ANF	> 10 ⁻⁵ (3)	> 10 ⁻⁵ (3)	ND
CNP-22	> 10 ⁻⁵ (3)	> 10 ⁻⁵ (3)	ND

^a p<0.05 versus rANP

^b p<0.01 versus rANP

Table 3: Residues interactions in the peptide-bound hNPRA-ECD complexes. Interactions

analysis was performed using the software SYBYL, as described under Materials and Methods.

Residues in each subunit of the ECD homodimer are specified as belonging to subunit A or B.

rANP7-27	Sites	BANP	Sites	A71915	Sites
		S1	D177a		
		L2			
		R3	L112a,M173a,D177a		
		R4	D192b		
		S5			
		S6	F172a,R176a	R6	F172a
C7		C7	H185a	C7	H185a
F8	Y154a,F165a,V168a, E169a,F172a,M173a, H185a	F8	Y154a,F165a,V168a, E169a,F172a,M173a	Cha8	Y154a,F165a,V168a, E169a,F172a,H185a
G9	M173a	G9	M173a	G9	M173a
G10	L112a,E169a,M173a	R10	M173a	G10	M173a
R11	L112a,G113a,V116a, E169a,M173a	R11	Y156b,E187b	R11	E187b,Y156b,E162b
I12		L12	Y88b	I12	F165a
D13	V87a,A91a,G113a, Y120a	D13	A91a,R95a,G113a, Y120a	D13	G113a,Y120a
R14	R95a,E119a,D62b, Y88b,Y120a	R14	A91a,R95a,D62b, Y88b	R14	D62b,R95a
I15	D62b,Y88b,A91b, P92a,P92b,R95a, R95b	I15	Y88a,F165a,F166a	I15	Y88b
G16	Y88a	G16	Y88a	D-tic16	V87b,Y88b, A111b, F165b,F166b,E169b
A17		S17	D62a,R95b,E119b, Y120b	R17	Y156a,P158a,E162a, F165b
Q18	A91b,G113b,F114b, F166b	L18	A111b,G113b,F114b, F116b,Y120b	C18-NH₂	F165b
S19	Y156a	S19			
G20	F165b,E169b	G20	L112b,F165b,E169b, M173b		
L21	F172b,M173b	L21	M173b		
G22	H185b	G22	F165b		
C23	H185b	C23			
N24	H185b,L186b,E187b	N24	Y154b,E187b		
S25	L186b,E187b	S25	H185b		
F26	H195b,R198b	F26	H185b,L186a,E187a		
R27	M173a,H195b	R27	Y154a,E187a		
		Y28	F172b,M173b,R174b, V175b,176b,D177b, V183b,H185b		

Figure 1

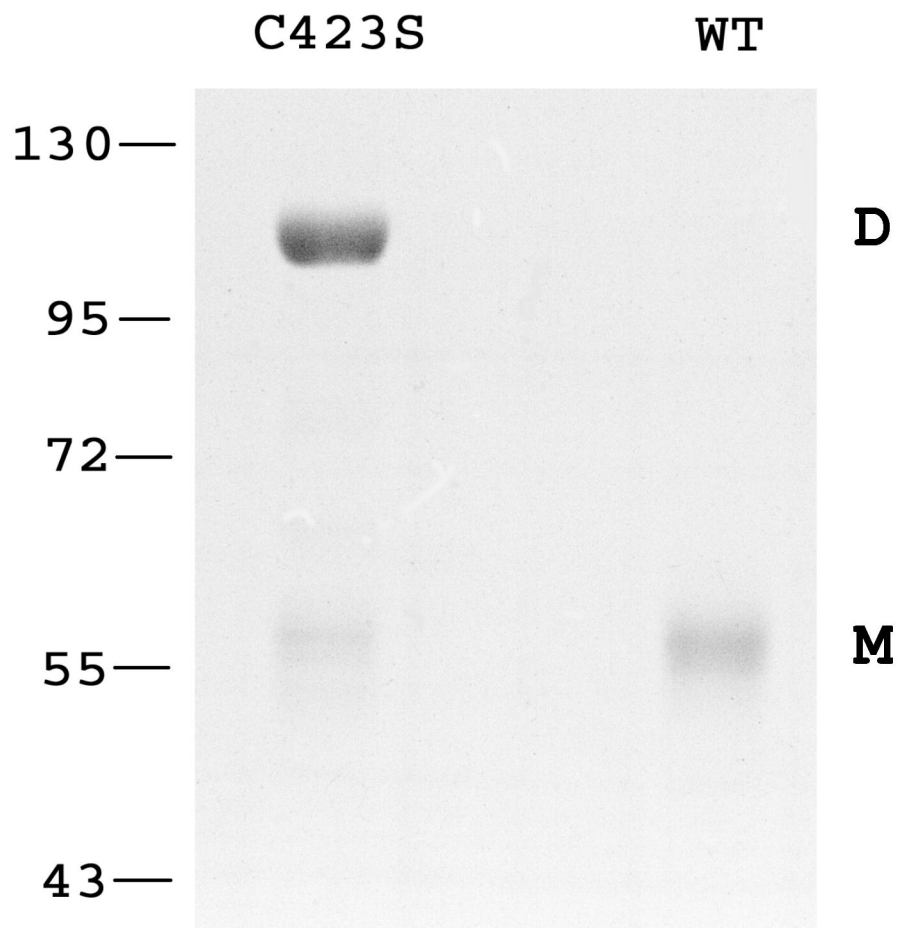
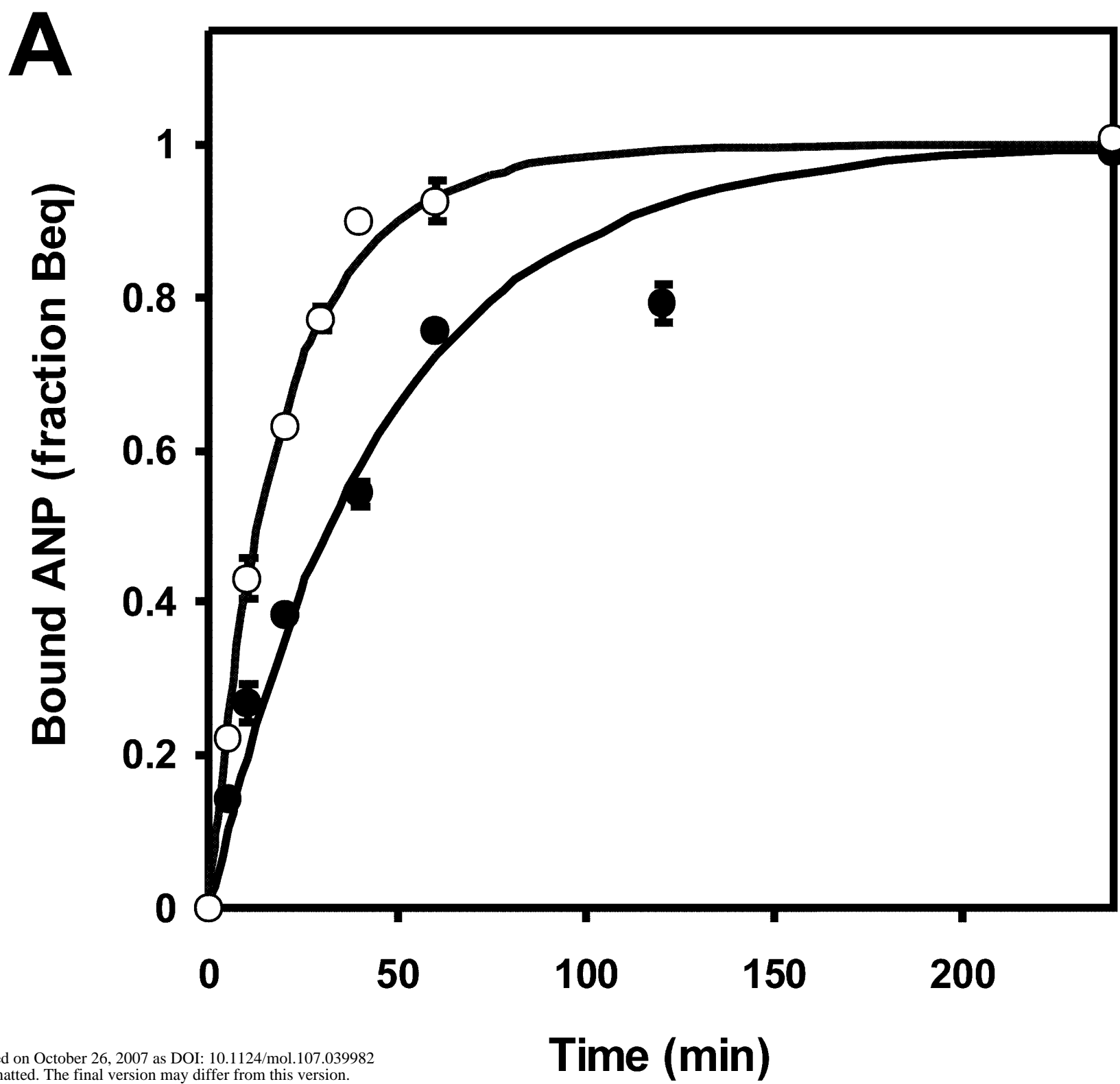


Figure 2



Molecular Pharmacology Fast Forward. Published on October 26, 2007 as DOI: 10.1124/mol.107.039982
This article has not been copyedited and formatted. The final version may differ from this version.

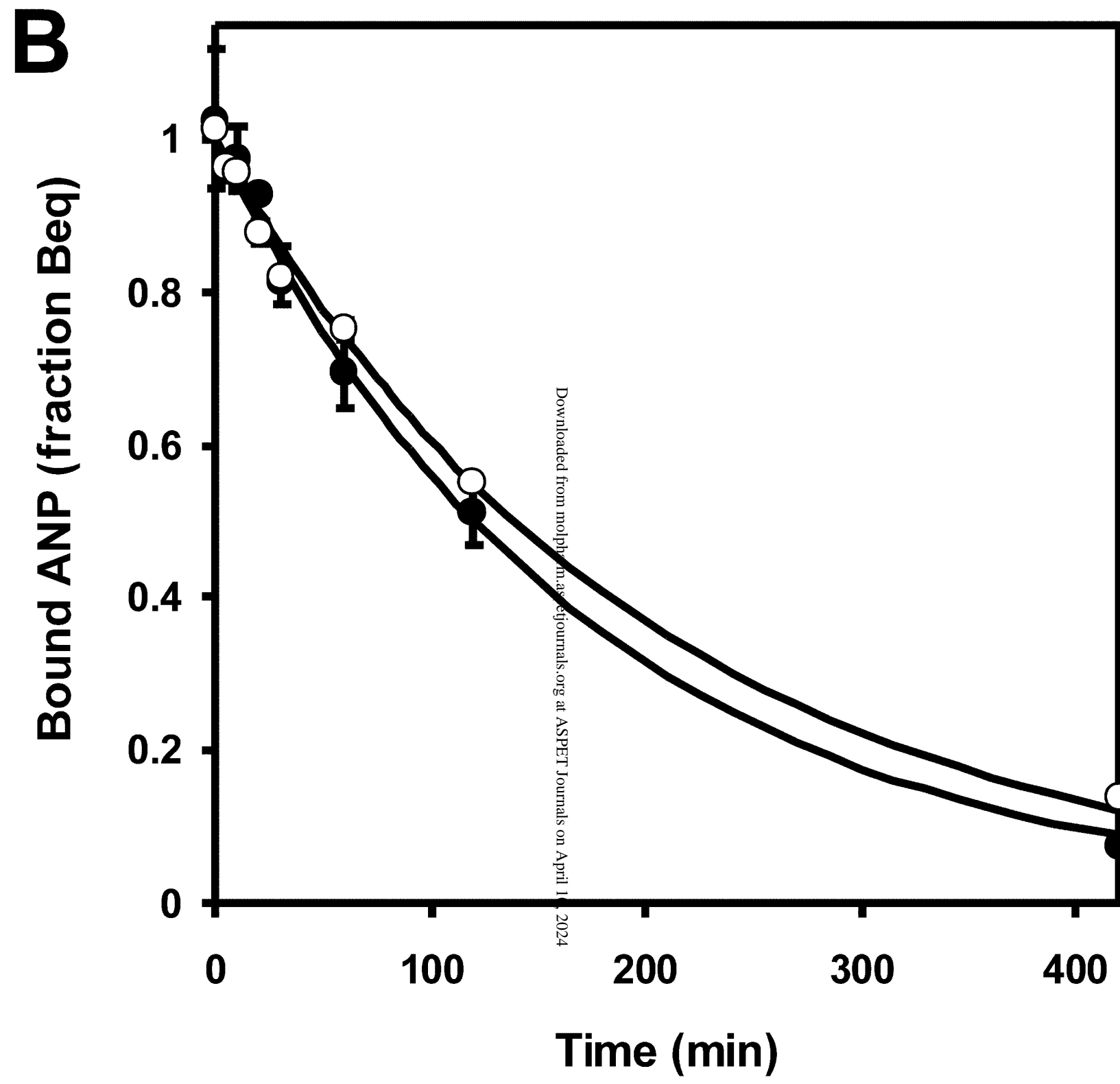


Figure 3

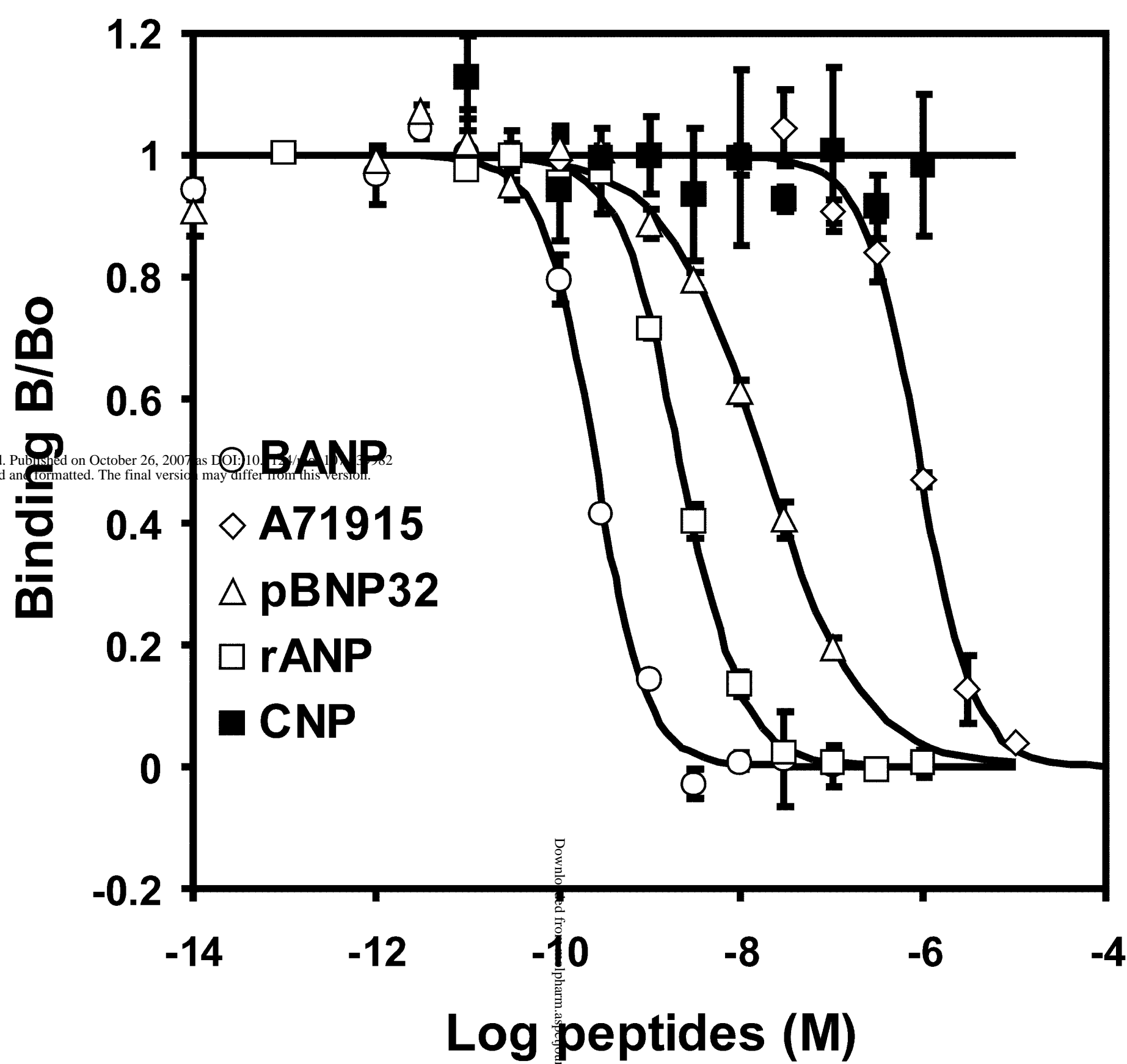
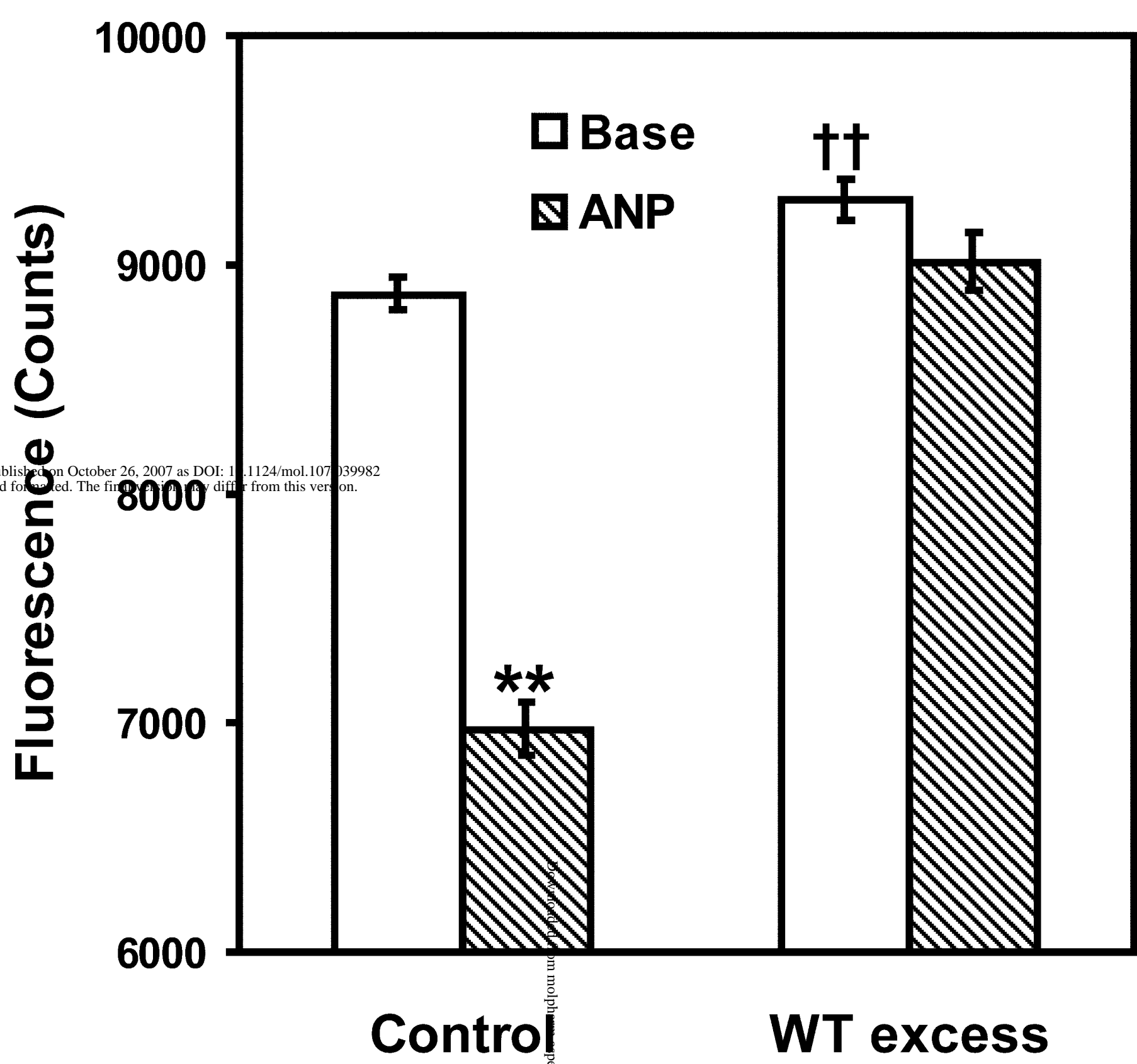
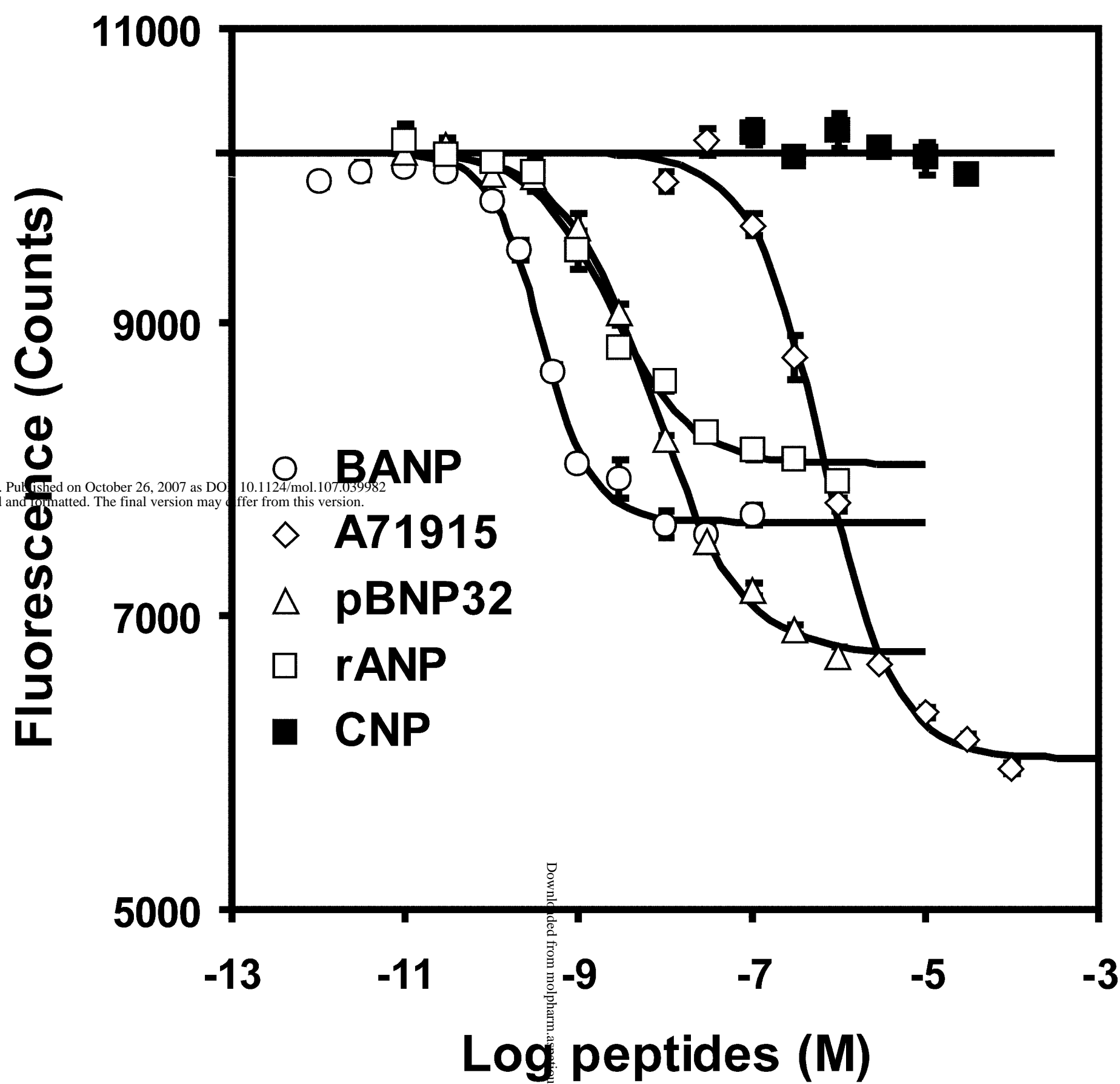


Figure 4



Molecular Pharmacology Fast Forward. Published on October 26, 2007 as DOI: 10.1124/mol.107.039982
This article has not been copyedited and formatted. The final version may differ from this version.

Figure 5



Molecular Pharmacology Fast Forward. Published on October 26, 2007 as DOI: 10.1124/mol.107.039982
This article has not been copyedited and formatted. The final version may differ from this version.

Figure 6

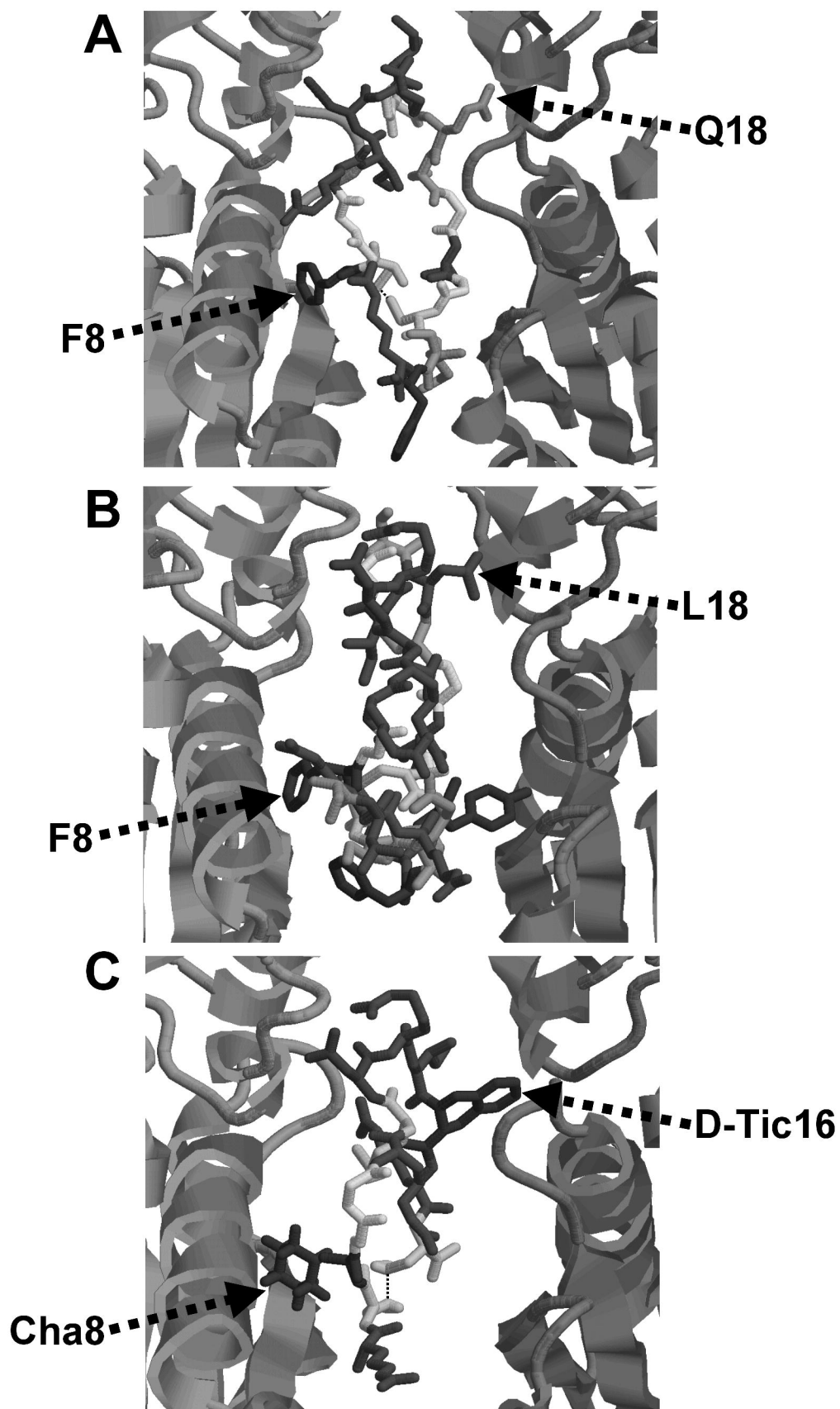


Figure 7

